Spatial and temporal luminescence dynamics in an $In_xGa_{1-x}N$ single quantum well probed by near-field optical microscopy

Akio Kaneta,[a] Koichi Okamoto, Yoichi Kawakami, and Shigeo Fujita
Department of Electronic Science and Engineering, Kyoto University, Kyoto 606-8501, Japan

Giichi Marutsuki, Yukio Narukawa, and Takashi Mukai
Nichia Corporation, 491 Oka, Kaminaka, Anan, Tokushima, 774-8601 Japan

(Received 18 June 2002; accepted 14 October 2002)

Spatial distribution of photoluminescence (PL) with spectral, spatial, and/or time resolution has been assessed in an $In_xGa_{1-x}N$ single-quantum-well (SQW) structure using scanning near-field optical microscope (SNOM) under illumination-collection mode at 18 K. The near-field PL images revealed the variation of both intensity and peak energy in PL spectra according to the probing location with the scale less than a few hundredths of a nanometer. PL linewidth, the value of which was about 60 meV in macroscopic PL, was as small as 11.6 meV if the aperture size was reduced to 30 nm. Clear spatial correlation was observed between PL intensity and peak wavelength, where the regions of strong PL intensity correspond to those of long wavelength. Time-resolved SNOM–PL study showed the critical evidence that supports the model of diffusion of carriers to potential minima. © *2002 American Institute of Physics.* [DOI: 10.1063/1.1526917]

Current progress in the fabrication technology of $In_xGa_{1-x}N/GaN/Al_yGa_{1-y}N$ heterostructures has led to the achievement of near ultraviolet, violet, blue, green, and amber light emitting diodes.[1–3] Two models have been reported so far to account for luminescence dynamics of an InGaN quantum well structure. The first one is that incorporation of In to Ga site is effective for suppressing nonradiative recombination centers related to point defects.[4] Another one is the effect of exciton localization induced by compositional fluctuation of In, where the pathways of nonradiative recombination centers are hindered once excitons are captured at potential minima.[5,6]

Several reports have recently been appeared on the spatial mapping of luminescence in $In_xGa_{1-x}N$ single-quantum wells (SQWs) by cathodoluminescence,[7–9] or by photoluminescence (PL) using scanning-near field optical microscopy (SNOM).[10–18] Most of the SNOM results were obtained using an illumination-mode system, which is very difficult to know whether excitons and/or carriers producing PL are directly photogenerated at the probe region or they are diffused from outside. This problem can be overcome by means of an illumination-collection mode[19] developed recently for the assessment of wide gap semiconductors.[15,16]

In this letter, the spatial inhomogeneiety and the temporal dynamics have been assessed at 18 K in a blue emitting $In_xGa_{1-x}N$ SQW by employing SNOM–PL and SNOM-time-resolved PL (TRPL) under the illumination-collection mode.

The sample is composed of sapphire (0002) substrate, a 1.5-μm-thick undoped-GaN, a 2.3-μm-thick n-type GaN:Si, a 3-nm-thick $In_xGa_{1-x}N$–SQW active layer ($x=$ about 0.2) and a 5-nm-thick undoped GaN layer. Macroscopic PL peak is located at about 490 nm at room temperature. The measurements were performed with NFS-300 near-field spectrometer developed at JASCO Corp. Two types of fibers were used in this study; double-tapered Ge-doped–SiO_2 cores with aperture diameter of 30 or 150 nm for detecting cw-PL, and single-tapered pure-SiO_2 cores with aperture diameter of 300 nm for detecting TRPL. An $In_xGa_{1-x}N$-based laser diode emitting at 400 nm (developed at Nichia Corp.) was used as the excitation source of cw–PL. PL signal collected by the fiber probe was introduced into a monochromator with spectral resolution of about 1 meV, and then detected by a cooled charge coupled device detector (Roper Scientific, Spec-10:400B/LN). For the TRPL measurement, the frequency-doubled mode-locked Al_2O_3:Ti laser emitting at 400 nm with the pulse width of 1.5 ps was used as an excitation source. A streak camera (Hamamatsu Photonics, C5680) was used as a detector.

Figure 1 shows the PL mapping plotted with PL peak intensity [(a)] as well as with PL peak wavelength [(b)] at 18 K under photoexcitation power density of 100 W/cm^2 using a 150 nm aperture fiber probe. It was found that the relative PL intensity fluctuates from 1 to 6, and that the PL peak

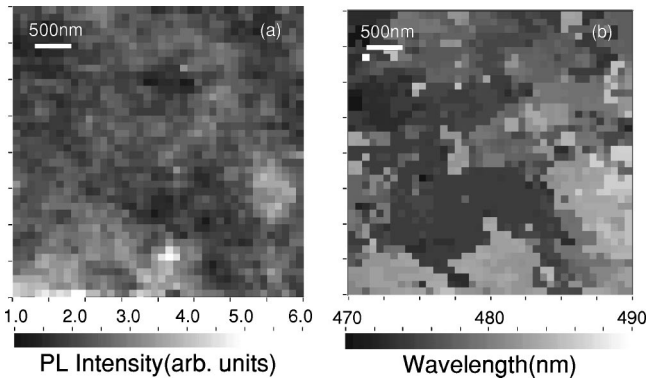

FIG. 1. Near-field PL image mapped with PL peak intensity (a) and peak wavelength (b) at 18 K. The excitation power density is 100 W/cm^2 cw condition. The scanning area is 4 μm×4 μm using a 150 nm aperture fiber probe.

[a]Electronic mail: kaneta@fujita.kuee.kyoto-u.ac.jp

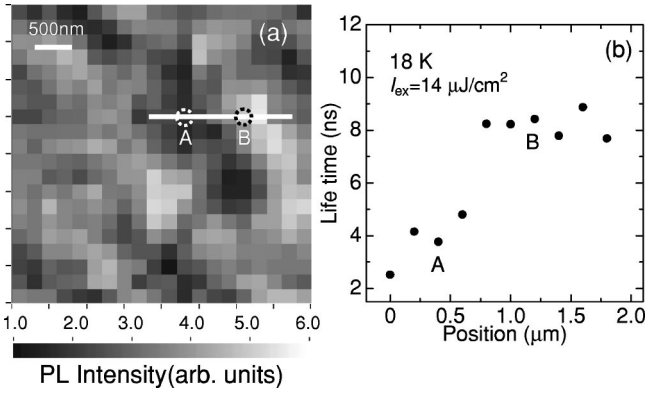

FIG. 2. (a) Near-field PL image mapped with PL peak intensity using a 300 nm aperture fiber probe at 18 K. (b) PL lifetimes plotted as a function of the position along the white bar shown in (a).

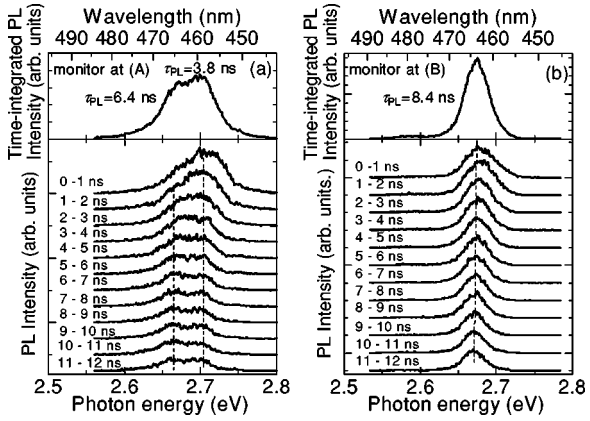

FIG. 3. Time-integrated PL and TRPL spectra as a function of time after pulsed excitation obtained at position A (a) and position B (b) at 18 K. (c) Decay spectra of PL intensity of position A and B.

wavelength is distributed from 470 to 490 nm, both of which consist of island-like structures within the range approximately 0.1–1 μm. A clear correlation was observed between the PL intensity and wavelength, where the areas of strong PL intensity correspond to those of long PL wavelength (small PL peak energy). Temperature dependence of macroscopic PL measurements reveals that the internal quantum efficiency (η_{int}) is nearly unity (0.9–1.0) below 100 K.[20,21] The PL peak intensity map [Fig. 1(a)] shows a relative intensity variation of approximately 1–6, corresponding to the η_{int} variation of 0.17–1.00 if the maximum is 1.00. If nonradiative recombination alone explained the spatial variation, then the spatially averaged quantum efficiency is estimated to be 0.41 taking into account the area of each PL intensity. This value is much smaller than unity that is the macroscopic η_{int} as mention earlier. Therefore, nonradiative recombination alone cannot explain the results; diffusion of carrers from the low-intensity to the high-intensity regions must occur.

In order to confirm such a mechanism, TRPL was employed under SNOM configuration. Figure 2(a) shows the PL-image mapped with the cw PL intensity taken with this fiber probe under 100 W/cm^2. TRPL was detected across the white bar drawn in the figure with the photoexcitation energy density is 14 μJ/cm^2. PL lifetimes of the emission peak are plotted as a function of position as shown in Fig. 2(b). It was found that the short lifetimes (2.5–4.8 ns) rapidly jump to the longer ones (7.6–9.0 ns) at about 0.75 μm. This position corresponds to the boundary where PL intensity changes from approximately 2.5 to 5.0. The PL lifetime (τ_{PL}) is expressed by the equation by, $1/\tau_{\mathrm{PL}}=1/\tau_{\mathrm{rad}}+1/\tau_{\mathrm{nonrad}}+1/\tau_{\mathrm{trans}}$, where τ_{rad} and τ_{nonrad} are radiative and nonradiative lifetimes, respectively, and τ_{trans} represents the transfer lifetime to lower lying energy levels arising from the localization phenomena. As mentioned earlier, the term of $1/\tau_{\mathrm{nonrad}}$ can be neglected at this temperature. Therefore, the shorter lifetimes at weak PL regions are contributed from the transfer lifetimes. This can be interpreted as PL peak energies of such regions are smaller than other surrounding regions. Figures 3(a) and 3(b) show the time-integrated PL, as well as time-resolved PL spectra as a function of time after pulsed excitation monitored at positions A and B, respectively. Time-integrated PL spectrum in Fig. 3(a) is composed of two-emission bands peaking at 458 and 464 nm. The main PL peak at 458 nm decays with the lifetime of 3.8 ns, while the longer peak at 464 nm does with 6.4 ns. However, for the Fig. 3(b), the PL band is composed of single emission peak associated with one LO-phonon replica, and decays with 8.4 ns. Two emission bands with different PL lifetimes in Fig. 3(a) are probably because the two regions having different energy levels are included within the probing aperture, and the excitons and/or carriers generated at the shorter wavelength region transfer to the longer wavelength regions distributed within or out of the aperture. Figure 4 shows the PL peak energies plotted as a function of excitation power under cw condition for two data points, namely for the weak intensity region [averaged 100 data point for smaller value than 25% of PL maximum intensity (I_{max})], and for the strong intensity regions (averaged 100 data point for larger value than 75% of I_{max}). The PL peak energy increases with increasing excitation power in both the strong intensity region and the weak intensity region. However, the blueshift is larger in the weak intensity region than in the strong intensity region for the same excitation intensity. These results can be explained by assuming that the density of states of localized levels decreases with increasing localization depth. Hence, more filling of the exciton and/or carrier band occurs in the weak intensity region than in the strong intensity region for the same excitation intensity. An additional factor that prob-

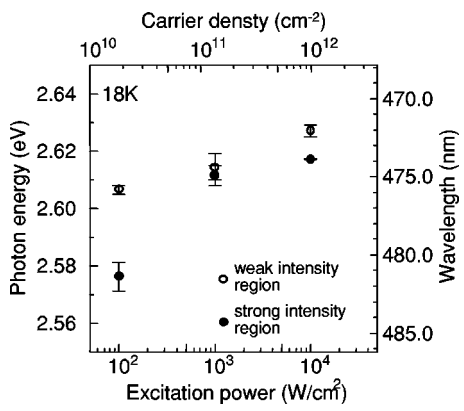

FIG. 4. PL peak energy as well as PL peak wavelength as a function of excitation power density at 18 K, averaged at weak PL intensity region, and at strong PL intensity region. The error bar shows the distribution of the data.

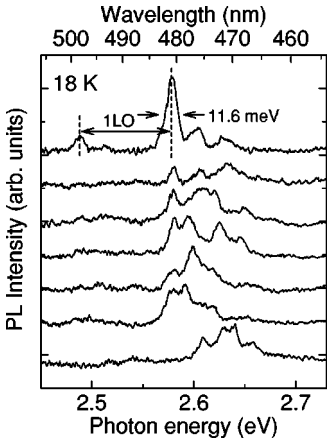

FIG. 5. Near-field PL spectra obtained at different positions using a 30 nm aperture fiber probe at 18 K. The excitation power density is 100 W/cm^2 cw conditions.

ably contributes to the blueshift in both regions is screening of the quantum well piezoellectoric field by the photogenetated excitons and/or carriers.

In order to assess the spatial distribution of localization centers, cw−PL was performed using a 30 nm aperture probe taken at different positions as shown in Fig. 5. Several peaks are clearly observed by using small aperture size fiber probe and the spectral shape is different form each other. The minimum PL linewidth is about 11.6 meV. This value is one fifth of macroscopic PL linewidth (about 60 meV), indicating that the macroscopic linewidth is not mainly contributed from the homogeneous broadening due to the interaction with phonon, but from the inhomogeneous one due to potential fluctuation.

The authors would like to thank Narita at JASCO Corp. for contributing the setup of SNOM. They are also grateful to Dr. Funato and Dr. Micheletto for valuable comments and discussion. This work was conducted by the Kyoto University-Venture Business Laboratory Project.

[1] S. Nakamura, M. Senoh, N. Iwasa, and S. Nagahama, Jpn. J. Appl. Phys., Part 2 **34**, L797 (1995).
[2] S. Nakamura, M. Senoh, N. Iwasa, S. Nagahama, T. Yamada, and T. Mukai, Jpn. J. Appl. Phys., Part 2 **34**, L1332 (1995).
[3] T. Mukai, H. Narimatsu, and S. Nakamura, Jpn. J. Appl. Phys., Part 2 **37**, L479 (1998).
[4] Y. Narukawa, S. Saijou, Y. Kawakami, S. Fujita, T. Mukai, and S. Nakamura, Appl. Phys. Lett. **74**, 558 (1999).
[5] S. Chichibu, T. Azuhata, T. Sota, and S. Nakamura, Appl. Phys. Lett. **69**, 4188 (1996).
[6] Y. Narukawa, Y. Kawakami, M. Funato, S. Fujita, and S. Fujita, Appl. Phys. Lett. **70**, 981 (1997).
[7] T. Sugahara, M. Hao, T. Wang, D. Nakagawa, Y. Naoi, K. Nishino, and S. Sakai, Jpn. J. Appl. Phys., Part 2 **37**, L1195 (1998).
[8] X. Zhang, D. H. Rich, J. T. Kobayashi, N. P. Kobayashi, and P. D. Dapkus, Appl. Phys. Lett. **73**, 1430 (1998).
[9] S. Chichibu, K. Wada, and S. Nakamura, Appl. Phys. Lett. **71**, 2346 (1997).
[10] P. A. Crowell, D. K. Young, S. Keller, E. L. Hu, and D. D. Awschalom, Appl. Phys. Lett. **72**, 927 (1998).
[11] A. Vertikov, M. Kuball, A. V. Nurmikko, Y. Chen, and S.-Y. Wang, Appl. Phys. Lett. **72**, 2645 (1998).
[12] A. Vertikov, A. V. Nurmikko, K. Doverspike, G. Bulman, and J. Edmond, Appl. Phys. Lett. **73**, 493 (1998).
[13] A. Vertikov, I. Ozden, and A. V. Nurmikko, Appl. Phys. Lett. **74**, 850 (1999).
[14] D. K. Young, M. P. Mack, A. C. Abare, M. Hansen, L. A. Coldren, S. P. Denbaars, E. L. Hu, and D. D. Awschalom, Appl. Phys. Lett. **74**, 2349 (1999).
[15] A. Kaneta, T. Izumi, K. Okamoto, Y. Kawakami, S. Fujita, Y. Narita, T. Inoue, and T. Mukai, Jpn. J. Appl. Phys., Part 1 **40**, 110 (2001).
[16] A. Kaneta, G. Marutsuki, K. Okamoto, Y. Kawakami, Y. Nakagawa, G. Shinomiya, T. Mukai, and S. Fujita, Phys. Status Solidi B **228**, 153 (2001).
[17] M. S. Jeong, Y.-W. Kim, J. O. White, E.-K. Suh, M. G. Cheong, C. S. Kim, C.-H. Hong, and H. J. Lee, Appl. Phys. Lett. **79**, 3440 (2001).
[18] J. Kim, K. Samiee, J. O. White, J.-M. Myoung, and K. Kim, Appl. Phys. Lett. **80**, 989 (2002).
[19] T. Saiki, K. Nishi, and M. Ohtsu, Jpn. J. Appl. Phys., Part 1 **37**, 1638 (1998).
[20] R. V. Miller, D. A. Kleinman, W. A. Nordland, Jr., and A. C. Gossard, Phys. Rev. B **22**, 863 (1980).
[21] K. Okamoto, S. Saijo, Y. Kawakami, M. Terajima, G. Shinomiya, T. Mukai, and S. Fujita, Rev. Sci. Instrum. (in press).